



Energy cost study for controlling complex social networks with conformity behaviorHong Chen  and Ee Hou Yong **Division of Physics and Applied Physics, School of Physical and Mathematical Sciences, Nanyang Technological University, Singapore 637371*

(Received 2 February 2021; revised 14 May 2021; accepted 2 June 2021; published 2 July 2021)

To understand controlling a complex system, an estimation of the required effort needed to achieve control is vital. Previous works have addressed this issue by studying the scaling laws of energy cost in a general way with continuous-time linear dynamics. However, continuous-time linear dynamics is unable to capture conformity behavior, which is common in many complex social systems. Therefore, to understand controlling social systems with conformity, discrete-time modeling is used and the energy cost scaling laws are derived. The results are validated numerically with model and real networks. In addition, the energy costs needed for controlling systems with and without conformity are compared, and it was found that controlling networked systems with conformity features always requires less control energy. Finally, it is shown through simulations that heterogeneous scale-free networks are less controllable, requiring a higher number of minimum drivers. Since the conformity-based model relates to various complex systems, such as flocking, or evolutionary games, the results of this paper represent a step forward toward developing realistic control of complex social systems.

DOI: [10.1103/PhysRevE.104.014301](https://doi.org/10.1103/PhysRevE.104.014301)**I. INTRODUCTION**

The controllability of complex networks have been studied extensively in recent years [1–14]. Owing to the ubiquity of networked systems in social [15], biological [16–18], ecological [19], technological [20], or financial [21] systems, understanding how to control them is important. The nodes of a network represent individual members, for example, species in an ecological network [15] or individuals in an opinion network [22], and links between nodes represent coupled interactions, for example, when a particular specie preys on the other, or when the opinion of an individual influences the opinion of others. Based on their complex networked interactions, complex dynamical systems could be modelled with state equations, where the states represent, for example, population level or support/opposition of a particular idea. Left to their own devices, these complex dynamical systems would evolve over time in a certain way. However, by introducing appropriate external interventions, the node states evolution could be altered (controlled) and made to behave in some other prescribed ways [1]. Therefore, by finding out which nodes in the network need to receive the appropriate external control signals (nodes which are injected with control signals are called driver nodes) [1,23], a complex system could be controlled and have its node states steered toward the desired final state vector.

Within the literature, particular attention has been paid toward the energy cost needed for control. The energy cost relates to the amount of effort that the drivers have to consume to steer the state vector, and is affected by the inverse of the

Gramian [24], which is dependent on the network structure, driver nodes, and control time T_f . Numerically, the energy cost has been studied in the context of optimization [25–28] and computation [29,30]. Analytically, scaling behaviors have been derived in terms of number of drivers [31], target nodes cardinality [32], and T_f [24,33,34].

While the aforementioned works have been adequate in their treatment of network control, the results presented have so far generalised the network dynamics to be continuous-time and linear, without taking into account conformity. Given that networked controllability is restricted to the study of networks with linear dynamics owing to the difficulty in controlling nonlinear dynamical systems [2], continuous-time linear dynamics modeling is unable to capture conformity, which are often nonlinear [35], the same way that discrete-time linear dynamics modeling can [36]. As shown in Ref. [36], when the dynamics of the networked system has conformity behavior, where each member adapts and mimics its nearest neighbors' node states, the results obtained can differ when comparing network dynamics with and without conformity. For example, the eigenvalues of unweighted chain, ring, and complete graphs differ when comparing the systems with and without conformity. Besides, the conclusions drawn from structural controllability using a generalized network structure were inconsistent when taking into account self-dynamics [4]. Further, conformity dynamics models a significant class of social systems in a more realistic way, which a generalised linear dynamics may fail to capture. For example, evolutionary games [37], learning behaviors [38,39] and collective movements [40–44] of animals are all described by models with conformity feature. Given the sensitivity of model specificities and the importance of control energy, it would be worthwhile to revisit previous calculations, keeping in mind conformity dynamics.

*eehou@ntu.edu.sg

In this paper, the energy cost needed to control a complex network with conformity behavior is studied. The idea behind this work is to check what are the effects of the mechanism of conformity on the energy cost. To do so, the energy cost is studied analytically through a series of scaling laws. In general, the energy cost is affected by several different parameters such as initial state vector, final state vector, final control time T_f , number of drivers, and even network eigenvalues. Therefore, a systematic study of the analytical scaling laws of the control energy is advantageous, as compared to numerical ones, because it characterizes exactly the boundaries of the energy cost based on these different parameters and allows the energy cost to be estimated. Based on the research results, it was found that for controlling networks with discrete-time linear dynamics and conformity behavior, the lower and upper bound energy cost scales as a function of T_f similarly to those of continuous-time linear dynamics without conformity behavior. While their scaling behaviors are similar, their energy costs are not. When comparing the energy cost needed to control systems with and without conformity, it was found that the energy cost of those with conformity features are always lower, suggesting that the mechanism of conformity is beneficial to the control of networked systems. Finally, the controllability of scale-free (SF) networks with degree-distribution $P(k) \sim k^{-\gamma}$ was also studied, and it was found that with or without conformity, the scaling exponent γ plays an important role in controllability, where SF networks with lower scaling exponent γ are less controllable, requiring a higher number of minimum driver nodes.

II. PROBLEM FORMULATION

In networked systems with conformity behavior, each node i mimics the strategies (or opinions) of its nearest neighbors j by adapting its node state in the next round as the average of its n_i nearest neighbors' node states in the current round [36]:

$$x_i(\tau + 1) = \frac{1}{s_i} \sum_{j=1}^{n_i} \hat{a}_{ij} x_j(\tau), \quad (1)$$

where $x_i(\tau)$ is the strategy of node i in discrete time τ , $s_i = \sum_{j=1}^N \hat{A}_{ij}$ is the weighted strength of node i , with $\hat{\mathbf{A}} = \{\hat{a}_{ij}\}$ being the $N \times N$ network matrix, where \hat{a}_{ij} is the directed weighted connection pointing from node j to node i , and zero otherwise. Note that x_i is a continuous variable that describes, for example, the degree of opinion in an opinion network [2,45], where a high x_i value indicate support for opinion A , and a low x_i value indicate support for opinion B . In evolutionary games, $x_i \in [0, 1]$ denotes the probability of node i to select a particular strategy. For example, $x_i = 1$ indicates that node i always chooses to cooperate, while with $x_i = 0$, node i always defects [36]. Equation (1) belongs to a class of conformity-based memory-one strategy games [46,47], where the strategy played by an agent is influenced only by the strategies of their immediate neighbors in the round prior. For example, a fair player has a weighted probability to cooperate with other players based their immediate neighbors' strategies played in the previous round [48].

Introducing input control signal terms to Eq. (1), and writing the state equation in vector notation, the complex system

has the following discrete linear time-invariant (LTI) dynamics [36]:

$$\begin{aligned} \mathbf{x}(\tau + 1) &= \mathbf{S}^{-1} \hat{\mathbf{A}} \mathbf{x}(\tau) + \mathbf{B} \mathbf{u}(\tau) \\ &= \mathbf{A} \mathbf{x}(\tau) + \mathbf{B} \mathbf{u}(\tau), \end{aligned} \quad (2)$$

where $\mathbf{x}(\tau) = [x_1(\tau), x_2(\tau), \dots, x_N(\tau)]^T$ is the state vector which captures the node states, $\mathbf{u}(\tau) = [u_1(\tau), u_2(\tau), \dots, u_M(\tau)]^T$ is the input control signals which attach to the complex network to alter the node states, $\mathbf{B} = \{b_{ij}\}$ is the $N \times M$ input matrix which tracks where the M number of control signals are placed, where $b_{ij} = 1$ if control signal j attaches to node i (nodes which receive control signals are called driver nodes), and $b_{ij} = 0$ otherwise, \mathbf{S}^{-1} is a $N \times N$ diagonal matrix with its nonzero entries as the inverse of weighted node strength s_i (if $s_i = 0$, then set $\mathbf{S}^{-1}(i, i) = 0$), $\mathbf{A} = \mathbf{S}^{-1} \hat{\mathbf{A}} = \{a_{ij}\}$ is the $N \times N$ network matrix with conformity behavior, and is in general nonsymmetric due to weighted quantity \mathbf{S}^{-1} .

Input control signal $\mathbf{u}(\tau)$ is responsible for driving the node states of the network and the energy cost required is defined as [34,49–51] $\mathcal{E}(T_f) = \sum_{\tau=0}^{T_f-1} \mathbf{u}^T(\tau) \mathbf{u}(\tau)$, where T_f is the final control time, which is the allocated time that control signal $\mathbf{u}(\tau)$ must complete its tasks. Minimizing the energy cost, the discrete-time energy-optimal control signal can be derived as [34,49]

$$\mathbf{u}^*(\tau) = \mathbf{B}^T (\mathbf{A}^T)^{T_f-\tau-1} \mathbf{W}^{-1} (\mathbf{x}_f - \mathbf{A}^{T_f} \mathbf{x}_0), \quad (3)$$

where

$$\mathbf{W}(T_f) = \sum_{\tau=0}^{T_f-1} \mathbf{A}^{T_f-\tau-1} \mathbf{B} \mathbf{B}^T (\mathbf{A}^T)^{T_f-\tau-1} \quad (4)$$

is the $N \times N$ discrete-time controllability Gramian matrix, $\mathbf{x}_0 = [x_1(0), x_2(0), \dots, x_N(0)]^T$ is the initial state vector and $\mathbf{x}_f = [x_1(T_f), x_2(T_f), \dots, x_N(T_f)]^T$ is the desired final state vector. Substituting $\mathbf{u}^*(\tau)$ into $\mathcal{E}(T_f)$, and assuming that $\mathbf{x}_0 = \mathbf{0}$, the cost function becomes $\mathcal{E}(T_f) = \mathbf{x}_f^T \mathbf{W}^{-1} \mathbf{x}_f$. In addition, to simplify the scope of the research, the final state vector \mathbf{x}_f is normalized by restricting the Euclidean distance $\mathbf{x}_f^T \mathbf{x}_f$ to be one, leading to the normalized cost function $E(T_f) = \mathcal{E}(T_f) / \mathbf{x}_f^T \mathbf{x}_f$, which is bounded by the eigenvalues of the Gramian using the Rayleigh-Ritz theorem [52]:

$$\frac{1}{|\eta'_{\max}[\mathbf{W}(T_f)]|} = \underline{E}' \leq E(T_f) \leq \bar{E}' = \frac{1}{|\eta'_{\min}[\mathbf{W}(T_f)]|}, \quad (5)$$

where \underline{E}' (\bar{E}') is the lower (upper) bound of the energy cost, and $|\eta'_{\max}(\mathbf{W})|$ ($|\eta'_{\min}(\mathbf{W})|$) is the absolute maximum (minimum) eigenvalue of Gramian \mathbf{W} . In other words, to calculate the lower and upper bound energy costs, it is crucial to compute the inverse of the absolute maximum and minimum eigenvalues of the controllability Gramian.

The controllability Gramian exists in simplified form, which has an analytical expression comprising the complex network's eigenvalues. This can be obtained through eigendecompositions $\mathbf{A} = \mathbf{P} \mathbf{D} \mathbf{P}^{-1}$ and $\mathbf{A}^T = \mathbf{V} \mathbf{D} \mathbf{V}^{-1}$, where $\mathbf{D}_{ii} = \lambda_i$ is the $N \times N$ diagonal matrix containing eigenvalues of \mathbf{A} (\mathbf{A}^T), sorted in ascending order of magnitude $|\text{Re}\lambda_1| \leq |\text{Re}\lambda_2| \leq \dots \leq |\text{Re}\lambda_N|$, and \mathbf{P} (\mathbf{V}) is the $N \times N$ associated eigenvectors of \mathbf{A} (\mathbf{A}^T). Substituting the eigendecompositions

into Eq. (4), the Gramian, expressed in Hadamard product form [24,31,33,34], becomes

$$\mathbf{W}(T_f) = \mathbf{P} \sum_{\tau=0}^{T_f-1} \mathbf{D}^\tau \mathbf{P}^{-1} \mathbf{B} \mathbf{B}^T \mathbf{V} \mathbf{D}^\tau \mathbf{V}^{-1} = \mathbf{P} \mathbf{M} \mathbf{V}^{-1}, \quad (6)$$

where $\mathbf{M}(T_f)$ is the simplified controllability Gramian, with (i, j) elements which can be obtained as (see Supplemental Material [53])

$$\mathbf{M}_{ij} = \mathbf{Q}_{ij} \frac{1 - (\lambda_i \lambda_j)^{T_f}}{1 - \lambda_i \lambda_j}, \quad (7)$$

with

$$\mathbf{Q}_{ij} = [\mathbf{P}^{-1} \mathbf{B} \mathbf{B}^T \mathbf{V}]_{ij}. \quad (8)$$

Therefore, to study the T_f scaling behaviors of normalized energy cost bounds, it suffices to analyze the eigenvalues of $\mathbf{M}(T_f)$ as T_f varies:

$$\frac{1}{|\eta_{\max}[\mathbf{M}(T_f)]|} = \underline{E} \leq E(T_f) \leq \bar{E} = \frac{1}{|\eta_{\min}[\mathbf{M}(T_f)]|}, \quad (9)$$

where \underline{E} (\bar{E}) is the lower (upper) bound of the energy cost, and $|\eta_{\max}[\mathbf{M}(T_f)]|$ ($|\eta_{\min}[\mathbf{M}(T_f)]|$) is the absolute maximum (minimum) eigenvalue of $\mathbf{M}(T_f)$.

While most eigenvalues are computed numerically, the eigenvalues of $\mathbf{M}(T_f)$ can be estimated analytically with the formulas [33,54]:

$$|\eta_{\max}[\mathbf{M}(T_f)]| \approx |\text{Re}[f(\bar{\alpha}, \bar{\beta})]| \quad (10)$$

and

$$|\eta_{\min}[\mathbf{M}(T_f)]| \approx \left| \text{Re} \frac{1}{f(\underline{\alpha}, \underline{\beta})} \right|, \quad (11)$$

where $f(\alpha, \beta) = \sqrt{\frac{\alpha}{N} + \sqrt{\frac{N-1}{N}(\beta - \frac{\alpha^2}{N})}}$, and

$$\bar{\alpha} = \text{trace}(\mathbf{M}^2), \quad (12)$$

$$\bar{\beta} = \text{trace}(\mathbf{M}^4), \quad (13)$$

$$\underline{\alpha} = \text{trace}[(\mathbf{M}^{-1})^2], \quad (14)$$

and

$$\underline{\beta} = \text{trace}[(\mathbf{M}^{-1})^4] \quad (15)$$

are pertinent estimation parameters for obtaining analytical \underline{E} or \bar{E} .

In subsequent analyses, through the use of Eqs. (10) and (11), the analytical scaling behaviors of the energy bounds with respect to T_f are given in terms of small and large T_f regime, and different number of driver nodes. Where possible, analytical estimations for \underline{E} and \bar{E} are made, if not, then approximate, or numerical ones, which are all validated against numerical computations of \underline{E} and \bar{E} .

III. RESULTS

In this section, for the first time, the energy cost scaling laws of a complex network with discrete-time linear dynamics and conformity behavior is derived and quantified using the estimation formulas Eqs. (10) and (11). Necessarily, because

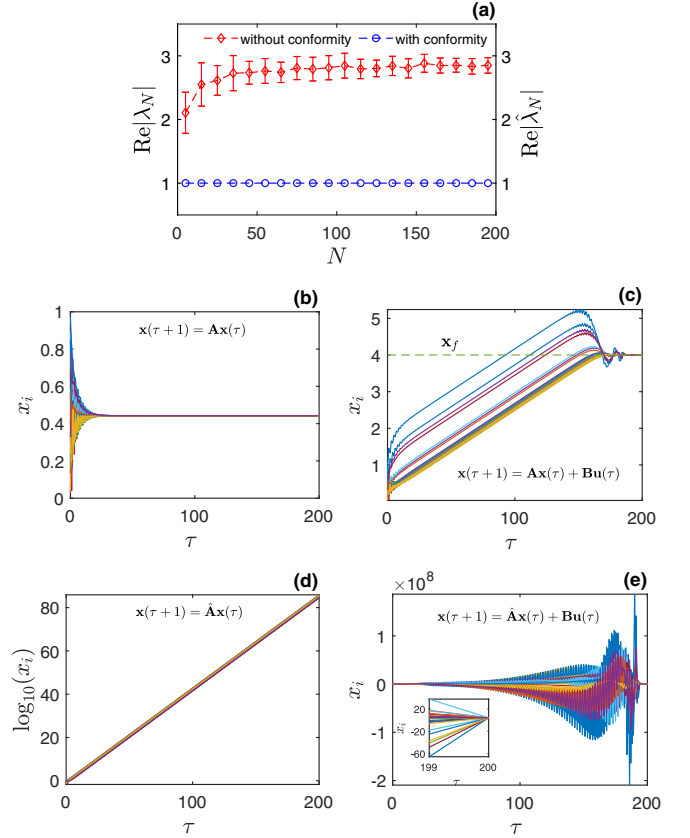


FIG. 1. Comparison of nonconformity and conformity discrete LTI models. The magnitudes of the largest eigenvalues of $\hat{\mathbf{A}}$ and \mathbf{A} denoted by $\text{Re}|\hat{\lambda}_N|$ and $\text{Re}|\lambda_N|$, respectively, for random network with fixed $\langle k \rangle = 4$ and varying N is shown in panel (a), where each data point is computed as the mean (error bars are standard deviation) of 20 independent network realizations. State equation evolving in τ with conformity dynamics, absent control $\mathbf{u}(\tau)$ is shown in panel (b), while panel (c) shows the node states being driven by one driver node toward the desired $\mathbf{x}_f = \mathbf{4}$. Panel (d) depicts the state equation of nonconformity dynamics, which is unstable and diverges in τ . Panel (e) demonstrates the unstable system being driven by one driver node toward $\mathbf{x}_f = \mathbf{4}$, with inset showing the final two time step.

the energy cost is somehow related to the network's eigenvalues, a discussion about the properties of the eigenvalues with and without conformity, and how they relate to system dynamics is given. Next, the energy costs needed to control complex networks with and without conformity are compared. Finally, the controllability properties of a SF network is studied, where it is showed, for the first time, that the scaling exponent γ of a SF network tunes its controllability.

The energy cost bounds are estimated analytically using Eqs. (10) and (11), which are themselves dependent on Eqs. (12)–(15), whose calculations depend on the traces of \mathbf{M} and \mathbf{M}^{-1} . Recalling Eq. (7), \mathbf{M}_{ij} is dependent on λ_i (and λ_j), the eigenvalues of network \mathbf{A} , which is why it is important to quantify λ_i , as the energy cost bounds are coupled to them. As an example, using undirected Erdős–Rényi (ER) random networks with average degree $\langle k \rangle = 4$ varying from system size $N = 5$ up to $N = 195$, it is shown in Fig. 1(a), that when the system has conformity behavior, $|\text{Re}\lambda_i| < 1$ for

$i = 1, 2, \dots, N - 1$, with $|\text{Re}\lambda_N| = 1$. In contrast, for the same network structure, but without conformity behavior, let the system dynamics be

$$\mathbf{x}(\tau + 1) = \hat{\mathbf{A}}\mathbf{x}(\tau) + \mathbf{B}\mathbf{u}(\tau), \quad (16)$$

where $\hat{\mathbf{A}}$ is the network structure without conformity, with eigenvalues $\hat{\lambda}_i$ (for $i = 1, 2, \dots, N$), then it can be seen from Fig. 1(a) that $\hat{\mathbf{A}}$ has maximum eigenvalue $|\text{Re}\hat{\lambda}_N| > 1$, which makes the discrete-time system unstable because the node states diverge in time. In practice, an unstable system is undesirable and stability is the basic requirement for control [55]. Thus, when the discrete-time system has conformity, the network's eigenvalues change and become less than or equal to one, causing the system to be stable and controllable.

To demonstrate system stability and instability, the evolutions of node states in an ER network with $N = 25$, and $\langle k \rangle = 4$, with and without conformity are plotted in Figs. 1(b) and 1(d), with \mathbf{x}_0 drawn from random uniform $[0,1]$. In Fig. 1(b), when each node i adapts its opinion as the average of its n_i nearest neighbors, over time, consensus is reached within the network. However, when there is no conformity behavior, it can be seen in Fig. 1(d) that opinions diverge in τ , owing to $\text{Re}|\hat{\lambda}_N| > 1$.

Regardless of system stability, both types of networks can be (numerically) controlled with one driver node. Setting $\mathbf{x}_f = [4, 4, \dots, 4]^T$, and using energy-optimal control signal $\mathbf{u}^*(\tau)$, with $\hat{\mathbf{A}}$ replacing \mathbf{A} in Eq. (3) for controlling network $\hat{\mathbf{A}}$, it is shown in Figs. 1(c) and 1(e) that the node states could be driven toward \mathbf{x}_f . However, due to system instability, control signal $\mathbf{u}(\hat{\mathbf{A}}, \tau)$ has to work much harder to bring the state vector toward the desired \mathbf{x}_f . At $T_f = 8N$, the numerical energy cost difference between controlling the system with and without conformity is about 15 orders of magnitude. While both conformity and nonconformity systems can be numerically controlled, the node states of the unstable system reach at least several orders of magnitude, which may in practice be infeasible.

Next, keeping in mind that $\lambda_i \leq 1$, the bounded estimates for the energy cost needed in controlling networks with discrete-time conformity-based linear dynamics is presented in the sections that follow. Before proceeding, it is worth mentioning that for discrete-time dynamical systems, T_f cannot be below a certain value, \underline{T}_f ; otherwise, the controllability Gramian is not invertible, and the system is not controllable. Based on numerical experiments, it was found that when using N drivers, $\underline{T}_f = 1$; otherwise,

$$\underline{T}_f = \left\lceil \frac{N}{M} \right\rceil + 1, \quad (17)$$

where M is the number of control signals or driver nodes.

A. Lower bound \underline{E}

As indicated in Fig. 1(a), networks \mathbf{A} which have conformity behavior all have $|\text{Re}\lambda_N| = 1$, with the rest of the eigenvalues $\lambda_i < 1$ for $i = 1, 2, \dots, N - 1$. Therefore, since $\mathbf{M}_{ij} = \mathbf{Q}_{ij} \frac{1 - (\lambda_i \lambda_j)^{T_f}}{1 - \lambda_i \lambda_j}$, all $(\lambda_i \lambda_j)^{T_f}$ terms vanish in the large T_f limit, with the exception of the last row/col element (using L'hopital's rule to evaluate the limit)

$\mathbf{M}_{NN} = \lim_{\text{Re}\lambda_N^2 \rightarrow 1} \mathbf{Q}_{NN} \frac{1 - \text{Re}(\lambda_N^2)^{T_f}}{1 - \text{Re}\lambda_N^2} = \mathbf{Q}_{NN} T_f$. In the large T_f limit, all \mathbf{M}_{ij} values are small relative to \mathbf{M}_{NN} , which dominates, and applying Eq. (10),

$$\underline{E} \approx \text{Re} \left| \frac{1}{\mathbf{Q}_{NN} T_f} \right| \sim T_f^{-1}, \quad (18)$$

regardless of number of drivers, which is validated with model networks (ER and SF) as shown in Fig. 2, and real networks (office [56] and karate [57]) as shown in Fig. 3. Note that the scaling $\underline{E} \sim T_f^{-1}$ is true for large T_f , but not necessarily true for small T_f . For small T_f , analytical \underline{E} should be estimated with Eqs. (10), (12), and (13) using the nonvanishing \mathbf{M}_{ij} . However, based on Figs. 2 and 3, $\underline{E} \sim T_f^{-1}$ approximates the small T_f lower bound energy cost with good agreement between analytical and numerical results in most cases. For Fig. 3(g), the deviation of the numerical computations from the analytical scaling is noticeable, and the small T_f analytical \underline{E} should be estimated with the nonvanishing \mathbf{M}_{ij} instead.

The driver nodes placement is encoded in \mathbf{Q} [Eq. (8)], which affects the simplified controllability Gramian \mathbf{M} [Eq. (7)], and is responsible for shifting the \underline{E} plots vertically. When controlling the network with a single control signal attached to node h , \mathbf{B} is a $N \times 1$ matrix, with entry $b_{h1} = 1$, and the rest of the elements $b_{ij} = 0$, leading to $\mathbf{B}\mathbf{B}^T = \mathbf{J}^{hh}$, where \mathbf{J}^{hh} is a single-entry matrix [58], and substituting into Eq. (8), $\mathbf{Q}_{ij} = [\mathbf{P}^{-1}]_{jh} v_{hi}$. When using d number of drivers (where $1 < d < N$), \mathbf{B} is a $N \times d$ matrix with the driver nodes placement $b_{ij} = 1$ if the j th control signal attaches to node i and zero otherwise, leading to $\mathbf{B}\mathbf{B}^T = \mathbf{J}^{d_1 d_1} + \mathbf{J}^{d_2 d_2} + \dots + \mathbf{J}^{d_d d_d}$, where d_k represents driver node k for $k = 1, 2, \dots, d$, then $\mathbf{Q}_{ij} = \sum_{k=1}^d [\mathbf{P}^{-1}]_{id_k} v_{d_k j}$. Finally, when controlling with all N drivers such that all N nodes each receive a control signal, \mathbf{B} is a $N \times N$ matrix with $b_{ii} = 1$ for $i = 1, 2, \dots, N$ and zero everywhere else, leading to $\mathbf{B} = \mathbf{I}$, and $\mathbf{Q}_{ij} = [\mathbf{P}^{-1}\mathbf{V}]_{ij}$. Consequently, substituting the resultant \mathbf{Q}_{ij} terms into Eq. (18),

$$\underline{E} \approx \begin{cases} |\text{Re}[\mathbf{P}^{-1}]_{Nh} v_{hN} T_f^{-1}|, & \text{one driver,} \\ |\text{Re}[\sum_{k=1}^d \mathbf{P}^{-1}]_{Nd_k} v_{d_k N} T_f^{-1}|, & d \text{ drivers,} \\ |\text{Re}[\mathbf{P}^{-1}\mathbf{V}]_{NN} T_f^{-1}|, & N \text{ drivers.} \end{cases} \quad (19)$$

Comparing Figs. 2(a)–2(c), 2(g)–2(i), and Figs. 3(a)–3(c), 3(g)–3(h), it can be seen that an increase in number of drivers leads to a decrease in \underline{E} .

B. Upper bound \bar{E}

Based on observing the numerical calculations of \bar{E} , there are two distinct regimes: small T_f regime, characterized by linear scaling behavior $\bar{E} \sim T_f^{-\Theta}$, where Θ is a numerical value to be found, and large T_f regime, where upper bound \bar{E} converge to a constant value. Using different number of driver nodes leads to different scaling exponents such that $\bar{E} \sim T_f^{-\Theta_1}$, $\bar{E} \sim T_f^{-\Theta_d}$, and $\bar{E} \sim T_f^{-\Theta_N}$ when using one driver, d drivers, and N drivers, respectively. Note that the range of small T_f regime is relatively small and decreases with increasing number of driver nodes. Small T_f regime is characterized

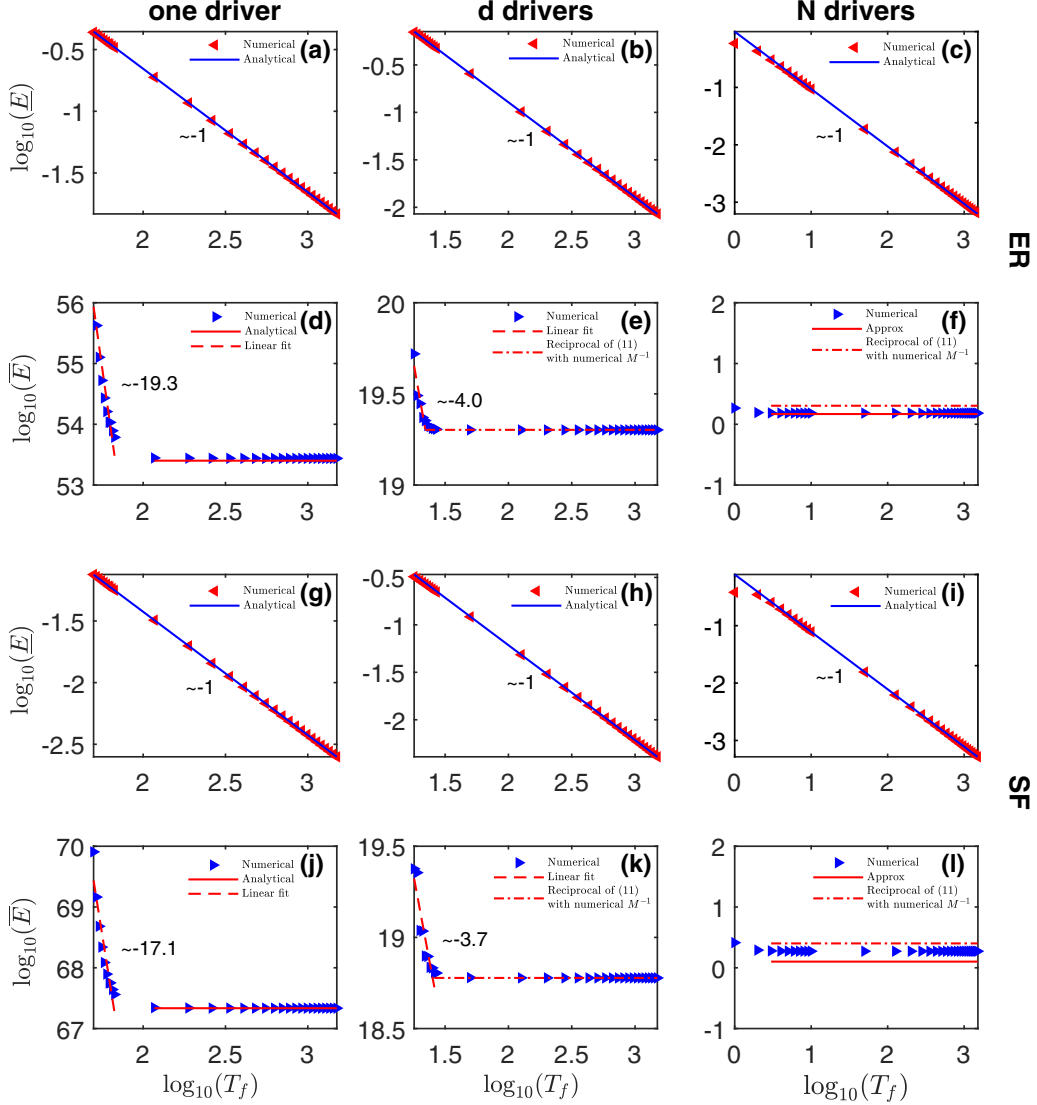


FIG. 2. Energy cost lower and upper bound for controlling model networks. Top-half (a–f) and bottom-half (g–l) panels relate to ER and SF networks (both are $N = 50$, $\langle k \rangle = 6$), respectively. Each column represents the same number of drivers, and $d = 3$. Triangles are numerical calculations of the inverse of maximum and minimum absolute eigenvalues of \mathbf{M} , while solid lines, dashed lines, and dash-dotted lines are respectively the analytical scaling laws, numerical linear fit, and \bar{E} estimates using Eq. (11), calculated from numerical \mathbf{M}^{-1} .

by the linear scaling behavior $\bar{E} \sim T_f^{-\Theta}$, and not by the range of T_f . A simple algorithm can be used to perform the linear fitting of numerical \bar{E} :

(1) Calculate numerical \bar{E} at $T_f = \{\underline{T}_f, \underline{T}_f + 1, \underline{T}_f + 2, \dots, \underline{T}_f + 9\}$, where \underline{T}_f is the minimum permissible T_f .

(2) Linear fit the first two data points computed at \underline{T}_f and $\underline{T}_f + 1$ and accept this range as the valid small T_f linear scaling regime.

(3) Linear fit the first three data points computed at \underline{T}_f , $\underline{T}_f + 1$, and $\underline{T}_f + 2$, and measure the R -squared value. If \bar{R} -squared value ≥ 0.85 , accept the data points as the valid small T_f linear scaling regime and move to step 4., else terminate.

(4) Repeat step 3. with increasing number of data points: linear fit \bar{E} computations evaluated at $T_f = [\underline{T}_f, \underline{T}_f + i]$, for $i = 3, 4, \dots, 9$.

From this simple algorithm, the small T_f regime is linearly fitted, where for one-driver-node calculations, small T_f regime spans several data points, which decreases as number of driver nodes increases. Because using one driver node requires the most control energy [31], it can be seen that $\Theta_1 > \Theta_d > \Theta_N$ when comparing Figs. 2(d)–2(f), 2(j)–2(l), and Figs. 3(d)–3(f), 3(i)–3(j). Θ_N is in general < 1 and essentially negligible in T_f . In addition, $\Theta_1 \sim \frac{N}{\langle k \rangle}$ regardless of network topology, as shown in Fig. 4.

Next, \bar{E} is derived for large T_f limit, when controlling the network with one driver node, where a control signal is attached to node h , leading to input matrix \mathbf{B} and simplified controllability Gramian matrix \mathbf{M} the same as before in Sec. III A. For the upper bound, analytical \bar{E} in the large T_f regime has to be estimated using Eqs. (11), (14), and (15), which are dependent on the inverse of the simplified controllability Gramian, \mathbf{M}^{-1} . While \mathbf{M} has an analytical

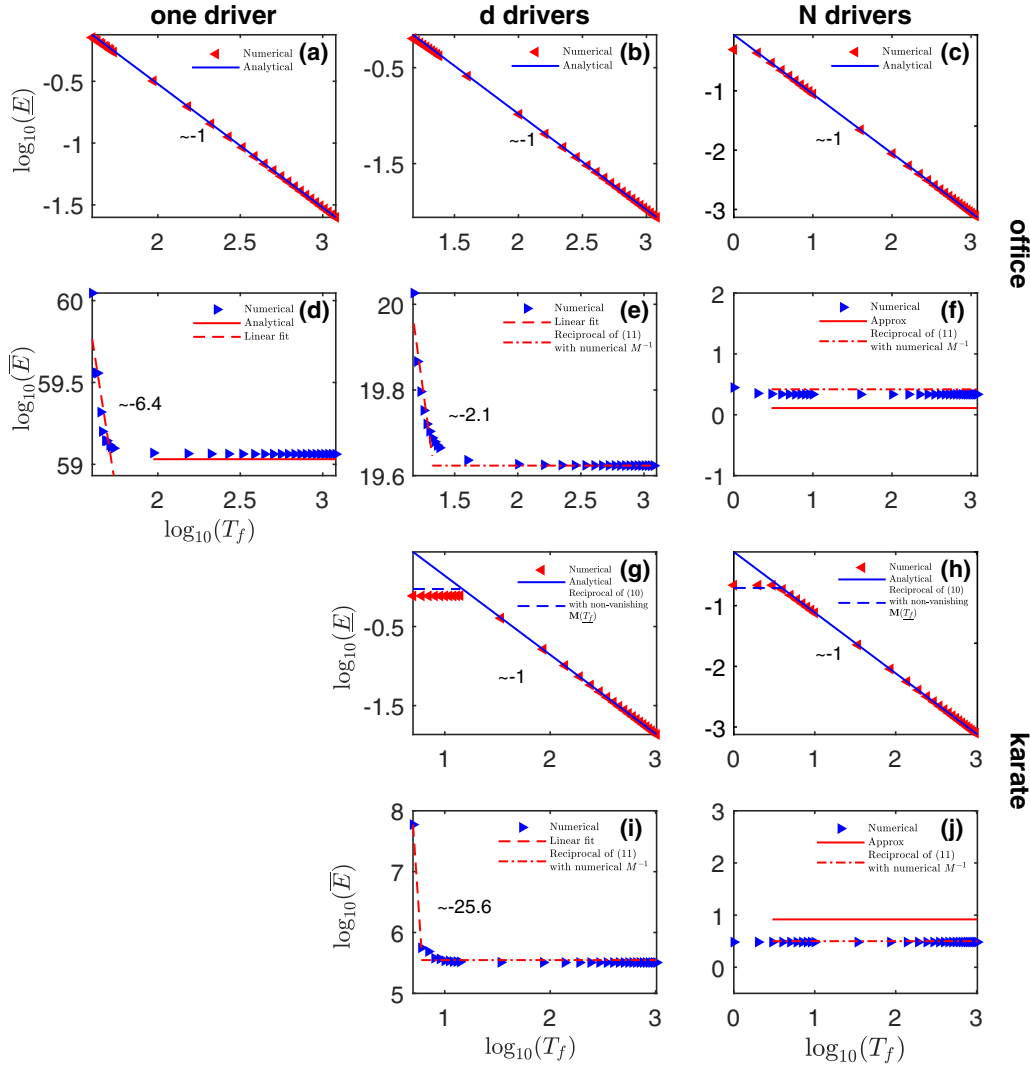


FIG. 3. Energy cost lower and upper bound for controlling real networks. Top-half (a–f) and bottom-half (g–j) panels relate to office and karate networks ($N = 40$, $\langle k \rangle = 11.9$, and $N = 34$, $\langle k \rangle = 4.6$), respectively. Each column represents the indicated number of drivers, with $d = 3$ for office network and $d = 10$ for karate network. There are no one-driver-node plots for karate network, because its minimum number of drivers [23] is $N_D = 10$. Triangles are numerical calculations of the inverse of maximum and minimum absolute eigenvalues of \mathbf{M} , while solid lines, red dashed lines, blue dashed lines, and dash-dotted lines are, respectively, the analytical scaling laws, numerical linear fit, small T_f analytical \underline{E} , and \bar{E} estimates using Eq. (11), calculated from numerical \mathbf{M}^{-1} .

expression as shown in Eq. (7), analytical \mathbf{M}^{-1} has to be derived by applying $\mathbf{M}^{-1} = \frac{\mathbf{M}^*}{|\mathbf{M}|}$, where \mathbf{M}^* is the adjoint matrix, and $|\mathbf{M}|$ is the determinant. Using Gaussian elimination to obtain the general expressions of \mathbf{M}^* and $|\mathbf{M}|$ based on \mathbf{M} , analytical \mathbf{M}^{-1} in the large T_f limit is obtained as shown in Eq. (B1). Note that Eq. (B1) differs nontrivially from Ref. [34]’s discrete-time system \mathbf{M}^{-1} , not just in terms of eigenvectors, but also in terms of form. Inspecting Eq. (B1), \mathbf{M}^{-1} elements lying in the last row/col are negligible when T_f is large. Ignoring those terms and applying Eq. (14), analytical $\underline{\alpha}$ Eq. (B2) is a constant. Similarly, $\underline{\beta}$ can be obtained through Eq. (15). Substituting $\underline{\alpha}$ and $\underline{\beta}$ into Eq. (11), analytical \bar{E} is a constant.

When using more than one driver (d and N drivers) to control the complex system, it is difficult to obtain analytical \mathbf{M}^{-1} in the large T_f limit. However, large T_f analytical \bar{E} can

still be estimated with Eqs. (11), (14), and (13) using \mathbf{M}^{-1} computed numerically. From Figs. 2 and 3, the \bar{E} scaling behavior of the system is noted to be the same as when using one driver node, and \bar{E} converge to a constant value in the large T_f limit. In addition, for N drivers, \bar{E} can also be approximated with Eq. (11) using an approximate analytical \mathbf{M}^{-1} , which is a diagonal matrix such that its nonzero entries $\mathbf{M}^{-1}(i, i) = [\mathbf{M}_{ii}]^{-1} = \frac{1-\lambda_i^2}{[\mathbf{P}^{-1}\mathbf{V}]_{ii}}$. This approximation can be verified against numerical computation of \mathbf{M}^{-1} , where it is noted that the main diagonal elements are large in comparison to the rest of matrix elements. Applying approximate \mathbf{M}^{-1} to Eqs. (14) and (15), $\underline{\alpha} \approx \sum_{i=1}^{N-1} \left[\frac{1-\lambda_i^2}{[\mathbf{P}^{-1}\mathbf{V}]_{ii}} \right]^2$ and $\underline{\beta} \approx \sum_{i=1}^{N-1} \left[\frac{1-\lambda_i^2}{[\mathbf{P}^{-1}\mathbf{V}]_{ii}} \right]^4$, which when applied to Eq. (11), also yields a constant in the large T_f limit. The validity of the analytical or approximate results are demonstrated in Figs. 2 and 3.

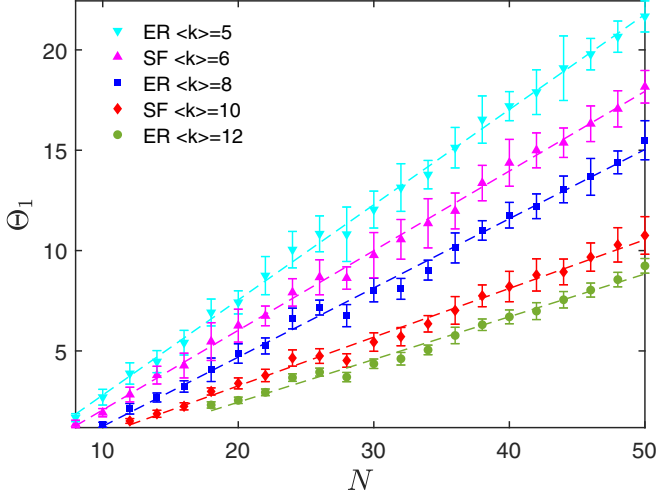


FIG. 4. Θ_1 calculated from numerical linear fit in small T_f regime of the one-driver scaling law, $\bar{E} \sim T_f^{-\Theta_1}$, for varying N and $\langle k \rangle$ with random and scale-free network topologies. Each data point is the mean of 20 independent network realizations and error bar is the standard deviation.

Regardless of network topology, it can be seen in Figs. 2 and 3 that the scaling behaviors of the upper bound \bar{E} of the energy cost with respect to T_f are very similar.

$$\bar{E} \begin{cases} \sim T_f^{-\Theta}, & \text{small } T_f, \\ \approx \text{constant}, & \text{large } T_f, \text{ one driver,} \\ \approx \text{constant}, & \text{large } T_f, d \text{ drivers,} \\ \approx \text{constant}, & \text{large } T_f, N \text{ drivers,} \end{cases} \quad (20)$$

where in the small T_f regime, because control signal $\mathbf{u}(\tau)$ has to drive the node states in a short amount of time, most energy is needed. Relaxing T_f requirement on the driver nodes reduces \bar{E} at a scaling rate of $\bar{E} \sim T_f^{\Theta_1}$, $\bar{E} \sim T_f^{\Theta_d}$, or $\bar{E} \sim T_f^{\Theta_N}$ depending on the number of drivers used. However, increasing T_f beyond a certain point, \bar{E} converge to a constant value. As expected, because increasing the number of drivers reduces control energy [31], \bar{E} is highest when using just one driver node.

C. Comparing large T_f \bar{E} : Conformity versus nonconformity

From Figs. 2, 3, and Eq. (20), it is apparent that \bar{E} scales $\sim T_f^{-\Theta}$ in the small T_f regime, eventually converging to a constant value in the large T_f limit. This behavior is similar to those of continuous-time dynamics [33], in particular, when the nonconformity continuous-time network $\tilde{\mathbf{A}}$ is not positive definite (PD, meaning that the eigenvalues of $\tilde{\mathbf{A}}$ are all positive) or positive semi-definite (PSD, meaning that the eigenvalues of $\tilde{\mathbf{A}}$ are all positive or zeros). A consequent natural question to ask is: How do the \bar{E} values compare in the absence and presence of conformity? Answering this question could offer insights into the mechanism of conformity in the context of networked controllability. Before proceeding, it is worth clarifying why only large T_f \bar{E} values should be compared between the conformity-based discrete-time dynamical system and the nonconformity-based continuous-time dynamical system. First, it is not sensible to compare conformity and

nonconformity dynamics energy costs between the discrete-time systems Eqs. (2) and (16) because while the former is stable, the latter is unstable. Second, it is not sensible to compare the energy costs in the small T_f regime, as the discrete-time dynamical system is limited by T_f , while the continuous-time dynamical system can set T_f to an arbitrarily small value. Third, it is not sensible to compare lower bound, as conformity-based \underline{E} goes to zero in the large T_f limit. It should be noted that T_f has different meaning in the discrete-time and continuous-time system; for example, $T_f = 20$ is a relatively small T_f for the discrete-time system, but $T_f = 20$ is a large enough value for the continuous-time system such that further increase in T_f would not lead to further reduction in energy cost [24,33]. For the remainder of this section, it can be assumed that the T_f values for the continuous-time or the discrete-time dynamical system are chosen sensibly such that only the convergent large T_f \bar{E} values are being compared.

The continuous-time dynamical system has the following dynamics [1]:

$$\dot{\mathbf{x}}(t) = \tilde{\mathbf{A}}\mathbf{x}(t) + \mathbf{B}\mathbf{u}(t), \quad (21)$$

where $\tilde{\mathbf{A}} = \{\tilde{a}_{ij}\} \in \mathbb{R}^{N \times N}$ describes the network connection such that when node j has a directed link to node i , a_{ij} is nonzero, otherwise, $a_{ij} = 0$, $\mathbf{B} = \{b_{ij}\} \in \mathbb{R}^{N \times M}$ accounts for where in the network the control signals are placed, for example, $b_{ij} = 1$ if control signal j attaches to node i , otherwise $b_{ij} = 0$, t is a continuous variable depicting instantaneous time, $\dot{\mathbf{x}}(t) = [\dot{x}_1(t), \dot{x}_2(t), \dots, \dot{x}_N(t)]^T$, $\mathbf{x}(t) = [x_1(t), x_2(t), \dots, x_N(t)]^T$, and $\mathbf{u}(t) = [u_1(t), u_2(t), \dots, u_N(t)]^T$ are, respectively, the instantaneous vector of rate of change of states, the state vector, and input control signals vector. Further, the continuous-time nonconformity network $\tilde{\mathbf{A}}$ is different from the discrete-time nonconformity network $\hat{\mathbf{A}}$ on the diagonal matrix elements. For the continuous-time system, to model system stability [31], $\tilde{a}_{ii} = \sum_{j=1}^N \tilde{a}_{ij} - \delta$, where δ represents a small perturbation to ensure system stability (in contrast, discrete-time $\hat{a}_{ii} = 0$). For the simulations that follow, $\delta = 0$, which is suitable for modeling opinion dynamics [45].

The energy cost for the continuous-time dynamical system is defined to be [59] $\mathcal{E}(T_f) = \int_0^{T_f} \mathbf{u}^T(t)\mathbf{u}(t)dt$, whereupon optimizing [24,33] leads to the continuous-time energy-optimal control signal

$$\mathbf{u}^*(t) = \mathbf{B}^T e^{\tilde{\mathbf{A}}^T(T_f-t)} \mathbf{W}^{-1} (\mathbf{x}_f - e^{\tilde{\mathbf{A}}T_f} \mathbf{x}_0), \quad (22)$$

where $\mathbf{W} = \int_0^{T_f} e^{\tilde{\mathbf{A}}(T_f-t)} \mathbf{B}\mathbf{B}^T e^{\tilde{\mathbf{A}}^T(T_f-t)} dt$ is the $N \times N$ continuous-time controllability Gramian, $\mathbf{x}_0 = [x_1(0), x_2(0), \dots, x_N(0)]^T$ is the initial state vector when $t = 0$, and $\mathbf{x}_f = [x_1(T_f), x_2(T_f), \dots, x_N(T_f)]^T$ is the final state vector at $t = T_f$ that the complex system is being driven toward. Following analogous reasoning as Sec. II, the bounds for the energy cost needed in controlling a continuous-time dynamical system is just the same as Eq. (9), except that η_{\min} and η_{\max} are the minimum and maximum eigenvalues of the simplified continuous-time controllability Gramian [33]:

$$\mathbf{M}(T_f) = \tilde{\mathbf{P}}^T \mathbf{W} \tilde{\mathbf{P}}, \quad (23)$$

where $\tilde{\mathbf{P}}$ is the eigenvectors matrix of the eigen-decomposed continuous-time nonconformity matrix $\tilde{\mathbf{A}} = \tilde{\mathbf{P}}\tilde{\mathbf{D}}\tilde{\mathbf{P}}^T$, and \mathbf{W} is the continuous-time controllability Gramian matrix. Thus,

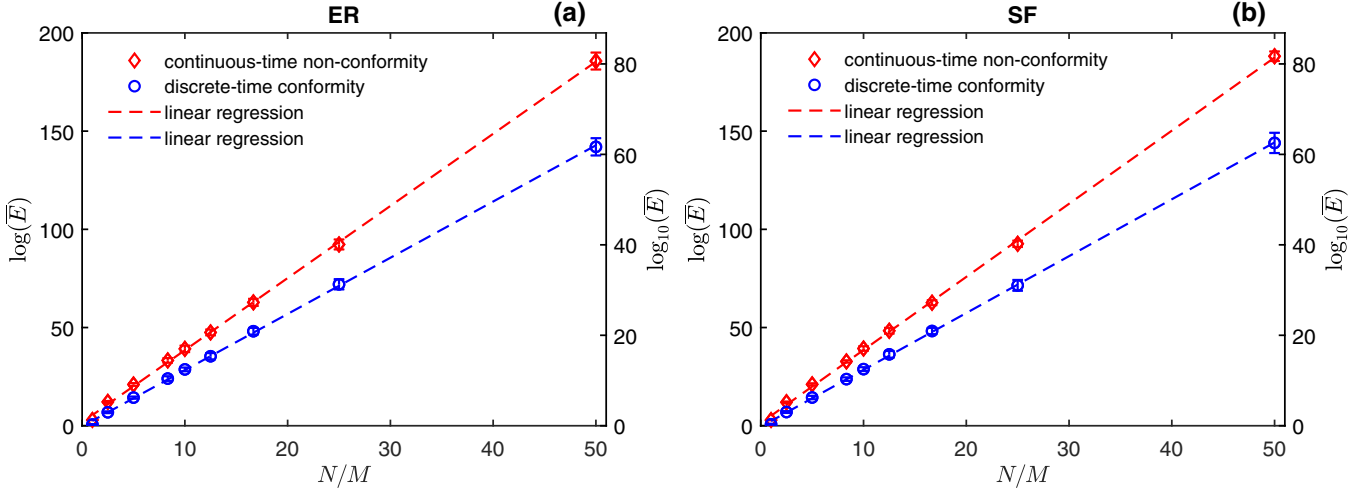


FIG. 5. Comparing the large T_f upper bound energy cost \bar{E} between the continuous-time nonconformity dynamical system and the discrete-time conformity-based dynamical system. The network sizes are all $N = 50$, with average degree of $\langle k \rangle = 8$. Both continuous-time nonconformity $\log(\bar{E})$ and discrete-time conformity $\log(\bar{E})$ can be linearly fitted against N/M , indicating that $\bar{E} \sim e^{N/M}$ for both types of systems. Overall, the conformity-based system requires less control energy. Panel (a) shows \bar{E} needed to control ER networks, while panel (b) shows \bar{E} needed to control SF networks. Each data point is computed based on the mean of 20 independent realizations, and error bars represent standard deviation.

numerically, the upper bound energy cost is computed as

$$\bar{E} = \frac{1}{|\eta_{\min}(\mathbf{M}(T_f))|}. \quad (24)$$

Computing large T_f \bar{E} for the continuous-time nonconformity and the discrete-time conformity systems, their energy costs are compared in Fig. 5. For both Figs. 5(a) and 5(b), corresponding to ER networks and SF networks, $\log(\bar{E})$ is plotted on the vertical axes, while N/M , the total N number of nodes of the complex network over the total M number of control signals, is plotted on their horizontal axes. For ease of reading the energy costs, the equivalent $\log_{10}(\bar{E})$ scale is also provided on the right-end vertical axes. Unsurprisingly, as noted from Fig. 5, the linear relationship between $\log(\bar{E})$ and N/M affirms the continuous-time results reported by Ref. [31], that the upper bound $\bar{E} \sim e^{N/M}$, indicating that an increase in the number of drivers leads to a decrease in maximum control energy at an exponential rate. Different from what has already been reported in the literature, however, is that this scaling behavior, $\bar{E} \sim e^{N/M}$, is also true for the discrete-time dynamical system with conformity. Further, regardless of number of drivers and complex network topology, the upper bound energy cost \bar{E} of the discrete-time conformity-based dynamical system always requires less control energy. When using only one control signal to drive the network such that $N/M = 50$, the difference in \bar{E} can be as much as 20 orders of magnitude. The disparity in \bar{E} lessens as the M number of drivers increases. The results suggest that the mechanism of conformity always leads to a complex system that is easier to control, requiring less control energy.

D. The role of scaling exponent γ in the controllability of SF networks

When computing N_D minimum number of drivers [23] needed to ensure controllability of the karate network in

Fig. 3, it was found that $N_D = 10$. Defining the degree of controllability as the fractional number of minimum drivers over the total number of nodes, $n_D = \frac{N_D}{N}$, and $\frac{\langle k \rangle}{N}$ as the density of connections of the network, the karate network was low in controllability (requiring high N_d to be controlled), with $n_D \approx 0.29$, despite being dense in connections $\frac{\langle k \rangle}{N} \approx \frac{4.6}{34} \approx 0.14$. In contrast, as shown in Ref. [36], SF networks with $\gamma = 3$ have n_D decreasing monotonically with increasing $\langle k \rangle$ toward $n_D = \frac{1}{N}$, where starting at $\frac{\langle k \rangle}{N} \approx \frac{3}{500} = 0.006$, are sufficiently dense and controllable with one driver. Therefore, with the karate network as a counterexample, $\langle k \rangle$ cannot be the only mechanism in determining the controllability of SF networks.

The scaling exponent γ also affects the controllability of SF networks. Using the static model [60] to generate SF networks with varying γ (where $2 < \gamma < \infty$), it is shown in Fig. 6, for fixed $N = 500$, that SF networks with lower γ (2.05) are less controllable. However, high γ (5 and 10) does not improve the controllability of SF networks significantly when compared to $\gamma = 3$. All scaling exponent γ curves display decreasing n_D with increasing $\langle k \rangle$, and the curves are the same without or without conformity dynamics.

IV. DISCUSSION

In this paper, the energy cost needed to control a complex network with conformity behavior is studied. To do so, a series of scaling laws were derived, based on the number of driver nodes, to characterize the control energy as a function of T_f in terms of its lower bound and upper bound, allowing for the energy cost to be estimated. A summary of the scaling laws can be found at Table I. In particular, it was found that lower bound scales as $\underline{E} \sim T_f^{-1}$, suggesting that in the large T_f limit, no energy cost is needed by the driver nodes to steer the state vector toward the least costly direction. If the intended final state vector coincides with the network consensus opinion, which can be reached naturally with conformity dynamics,

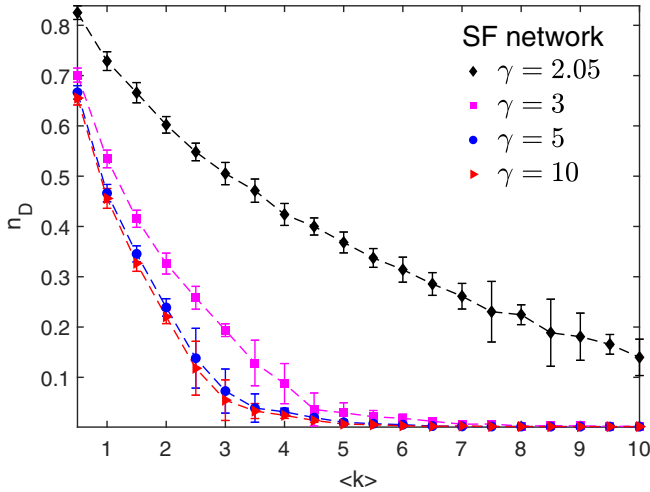


FIG. 6. The degree of controllability n_D of SF networks with varying γ and $\langle k \rangle$ values. Each data point is the mean of 20 independent network realizations, with the error bar being the standard deviation.

then no further action is required by the driver nodes. Upper bound energy cost decreases with increasing T_f at a rate of $\bar{E} \sim T_f^{-\Theta}$ in the small T_f limit, suggesting that in this regime, setting a relatively larger T_f always leads to less energy cost. Further, it was found that $\Theta_1 \sim \frac{N}{\langle k \rangle}$ regardless of network topology, and the small T_f regime scaling behavior depends only on system size and average node degree. In the large T_f limit, \bar{E} converges to a constant value, indicating that in this regime, the energy cost cannot be lowered any further by increasing T_f . Overall, these scaling laws have implications about the trade-off between final control time T_f and energy cost and is useful to the design of control strategies in complex social networks with conformity behavior.

It is interesting to note the difference in controllability and energy cost of the networked systems with and without conformity. From the point of view of dynamical systems, the discrete-time nonconformity model $\hat{\mathbf{A}}$ is always practically uncontrollable owing to system instability. Yet, the same network structure with conformity in discrete-time linear dynamics, $\mathbf{A} = \mathbf{S}^{-1}\hat{\mathbf{A}}$, is always stable and controllable, suggesting that the mechanism of conformity can make an otherwise unstable and uncontrollable discrete-time linear dynamical complex system stable and controllable. In terms of controllability, it was found that the fractional minimum number of drivers that guarantees the controllability of a SF network is unaffected by the mechanism of conformity.

TABLE I. Summary of the scaling behaviors of the lower bound \underline{E} and upper bound \bar{E} of the energy cost with respect to T_f in small and large T_f regime using one, d , and N number of drivers.

	T_f regime	One driver	d drivers	N drivers
\underline{E}	Small/large	$\sim T_f^{-1}$	$\sim T_f^{-1}$	$\sim T_f^{-1}$
\bar{E}	Small	$\sim T_f^{-\Theta_1}$	$\sim T_f^{-\Theta_d}$	$\sim T_f^{-\Theta_N}$
\bar{E}	Large	Eq. (11) with Eq. (B1)	Constant	Constant

Instead, given the scale-free degree distribution $P(k) \sim k^{-\gamma}$ of a SF network, it was found that the scaling exponent γ tunes the controllability, and heterogeneous (smaller γ) [61] SF networks are less controllable, requiring a higher minimum number of driver nodes. In terms of energy cost, networks with discrete-time linear dynamics and conformity behavior and networks with continuous-time linear dynamics but no conformity behavior both scale as a function of number of drivers as $\bar{E} \sim e^{N/M}$, indicating that regardless of conformity, adding more driver nodes always reduces the maximum control energy at an exponential rate. Nevertheless, comparing the convergent large T_f \bar{E} values of the different systems shows that the conformity-based model always requires less control energy with a difference of \bar{E} values by as much as 20 orders of magnitude when using one driver node to control networks of system size $N = 50$. All in all, the results suggest that the mechanism of conformity plays an important role in making a complex social system more controllable.

Objectively speaking, the degree to which a social system is controllable has neutral connotations: It is neither better nor worse to be more or less controllable. For example, a complex social system that is more difficult to control is at the same time more resilient against malicious social manipulations as it is against positive social change. The converse is true for a complex social system that is easier to control. Thus, from the point of view of governance, conformity behavior in complex social systems should be discouraged in some situations, for example, the sharing of controversial or polarizing news, and encouraged in some others, for example, the propagation of ideas which can lead to positive social change such as recycling. Recently, a few sociophysics works have been successful in corroborating their mathematical models with real world data, such as the distributions of agree, disagree, or undecided in controversial and noncontroversial topics using poll data [62], and the emergence of echo chambers in social networks surrounding politically controversial topics using Twitter data [63]. It would be interesting to corroborate or even disprove, with real world data, the claim of the present research that conformity in social networks always leads to a situation where the network is easier to control or influence. Further, a limitation of networked controllability is that only linear dynamics can be studied [2], while various socio-physics models can be nonlinear or have states which are not continuous variables [22]. In these types of models, how would conformity dynamics influence the system as a whole?

ACKNOWLEDGMENTS

The authors are grateful to Dr. Chew Lock Yue and Dr. Chiam Keng-Hwee for helpful discussion and suggestions, and Matthew Ho for guidance on creating high resolution figures from Matlab. H.C. and E.H.Y. acknowledge support from Nanyang Technological University, Singapore, under its Start Up Grant Scheme (Grant No. 04INS000175C230).

APPENDIX A: METHODS

System stability, network matrix diagonal entries and numerical precision require careful attention during compu-

tation. Unlike its continuous-time counterparts, which could be stabilized by introducing negative terms along the network diagonals [31], the discrete-time system cannot be stabilized the same way. Introducing diagonal entries in $\hat{\mathbf{A}}$ would cause system instability for both nonconformity and conformity discrete-time dynamics. Therefore, in this work, for discrete-time dynamics, the diagonal entries of $\hat{\mathbf{A}}$ are zero, and conformity-based model is stable with eigenvalues $\lambda_i \leq 1$. When computing the state equation of the unstable nonconformity discrete-time dynamics, which diverges, high numerical precision is needed, which can be achieved using Advanpix [64]. Computing the unstable state equation without high numerical precision, using the standard double precision, would lead to erroneous calculations where they would wrongly stabilize in large τ . Further, one-driver-node control typically requires high energy cost, and \bar{E} has to be calculated with high numerical precision.

The model networks used in this paper are constructed with the standard Erdős–Rényi random network algorithm, and the static model [60], where in Fig. 2, $\gamma = 2.5$, in Fig. 5, $\gamma = 3.0$, and in Fig. 6, γ is varied. All model networks $\hat{\mathbf{A}}$ and $\tilde{\mathbf{A}}$ are undirected, symmetric, and weighted, with link weights $\hat{a}_{ij} = \hat{a}_{ji}$ or $\tilde{a}_{ij} = \tilde{a}_{ji}$ drawn from random uniform

(0,1]. The network construction algorithms do not guarantee that the graph object does not have isolated nodes, and for one-driver-node calculations, checks were done to ensure that each node has at least one connection, otherwise the network was discarded and replaced. For the real networks, the karate network is unweighted with link $\hat{a}_{ij} = 1$ if nodes i and j are connected and zero otherwise, the office network is weighted but with integer \hat{a}_{ij} greater or equal to 1 if nodes i and j are connected and zero otherwise.

With sufficiently high average degree $\langle k \rangle$, the conformity-based model networks used have $N_D = 1$, and any random choice of driver nodes (for d drivers and one driver) would suffice to ensure network controllability. It should be noted that k , node degree, and s , node strength, are distinct from each other; where the former is calculated from the adjacency matrix, and the latter from $\hat{\mathbf{A}}$ whose links \hat{a}_{ij} are weighted. For computing minimum driver nodes [23], the Matlab software written by Patel was used [65].

APPENDIX B: ONE-DRIVER-NODE ANALYTICAL EQUATIONS

$$\mathbf{M}^{-1}(i, j) = \begin{cases} \frac{(-1)^N \prod_{k=1}^{N-1} (1 - \lambda_i \lambda_k) \prod_{l=1}^{N-1} (1 - \lambda_l \lambda_i)}{[\mathbf{P}^{-1}]_{jh} v_{hi} \prod_{k=1}^{N-1} (\lambda_i - \lambda_k) \prod_{l=1}^{N-1} (\lambda_l - \lambda_i)}, & i = j, (N-1) \times (N-1) \text{ block,} \\ \left[\frac{(-1)^{N+1}}{(\lambda_j - \lambda_i) v_{hi} [\mathbf{P}^{-1}]_{jh}} \right] \left[\frac{\prod_{k=1}^{N-1} (1 - \lambda_i \lambda_k) \prod_{k=1}^{N-1} (1 - \lambda_k \lambda_j)}{\prod_{k=1}^{N-1} (\lambda_i - \lambda_k) \prod_{k=1}^{N-1} (\lambda_k - \lambda_j)} \right], & i \neq j, (N-1) \times (N-1) \text{ block,} \\ \frac{1}{q_{NN} T_f} = \frac{1}{[\mathbf{P}^{-1}]_{Nh} v_{hN} T_f}, & i = j = N, \\ \left[\frac{(-1)^N}{[\mathbf{P}^{-1}]_{jh} v_{hi} (\lambda_j - \lambda_i) T_f} \right] \left[\frac{\prod_{k=1}^{N-1} (1 - \lambda_i \lambda_k) \prod_{l=1}^{N-1} (1 - \lambda_l \lambda_j)}{\prod_{k=1}^{N-1} (\lambda_i - \lambda_k) \prod_{l=1}^{N-1} (\lambda_l - \lambda_j)} \right], & i \neq j, N \text{th row/col.} \end{cases} \quad (\text{B1})$$

$$\begin{aligned} \underline{\alpha} &= \text{trace}[(\mathbf{M}^{-1})^2] \approx \sum_{i=1}^{N-1} \sum_{a=1}^{N-1} [\mathbf{M}^{-1}]_{ia} [\mathbf{M}^{-1}]_{ai} + [\mathbf{M}^{-1}]_{ii} [\mathbf{M}^{-1}]_{ii} \\ &\approx \sum_{i=1}^{N-1} \sum_{a=1}^{N-1} \left[\frac{1}{(\lambda_a - \lambda_i) v_{hi} [\mathbf{P}^{-1}]_{ah}} \right] \left[\frac{\prod_{k=1}^{N-1} (1 - \lambda_i \lambda_k) \prod_{k=1}^{N-1} (1 - \lambda_k \lambda_a)}{\prod_{k=1}^{N-1} (\lambda_i - \lambda_k) \prod_{k=1}^{N-1} (\lambda_k - \lambda_a)} \right] \left[\frac{1}{(\lambda_i - \lambda_a) v_{ha} P_{ih}^{-1}} \right] \\ &\quad \times \left[\frac{\prod_{k=1}^{N-1} (1 - \lambda_a \lambda_k) \prod_{k=1}^{N-1} (1 - \lambda_k \lambda_i)}{\prod_{k=1}^{N-1} (\lambda_a - \lambda_k) \prod_{k=1}^{N-1} (\lambda_k - \lambda_i)} \right] + \left[\frac{\prod_{k=1}^{N-1} (1 - \lambda_i \lambda_k) \prod_{l=1}^{N-1} (1 - \lambda_l \lambda_i)}{[\mathbf{P}^{-1}]_{ih} v_{hi} \prod_{k=1}^{N-1} (\lambda_i - \lambda_k) \prod_{l=1}^{N-1} (\lambda_l - \lambda_i)} \right]^2. \end{aligned} \quad (\text{B2})$$

See Supplemental Material for additional information [53].

- [1] Y.-Y. Liu, J.-J. Slotine, and A.-L. Barabási, Controllability of complex networks, *Nature* **473**, 167 (2011).
- [2] Y.-Y. Liu and A.-L. Barabási, Control principles of complex systems, *Rev. Mod. Phys.* **88**, 035006 (2016).
- [3] W.-X. Wang, X. Ni, Y.-C. Lai, and C. Grebogi, Optimizing controllability of complex networks by minimum structural perturbations, *Phys. Rev. E* **85**, 026115 (2012).
- [4] N. J. Cowan, E. J. Chastain, D. A. Vilhena, J. S. Freudenberg, and C. T. Bergstrom, Nodal dynamics, not degree distributions, determine the structural controllability of complex networks, *PLoS One* **7**, e38398 (2012).
- [5] J. Sun and A. E. Motter, Controllability Transition and Nonlocality in Network Control, *Phys. Rev. Lett.* **110**, 208701 (2013).
- [6] J. Gao, Y.-Y. Liu, R. M. D'souza, and A.-L. Barabási, Target control of complex networks, *Nat. Commun.* **5**, 5415 (2014).
- [7] F. L. Iudice, F. Garofalo, and F. Sorrentino, Structural permeability of complex networks to control signals, *Nat. Commun.* **6**, 8349 (2015).
- [8] A. J. Whalen, S. N. Brennan, T. D. Sauer, and S. J. Schiff, Observability and Controllability of Nonlinear Networks: The Role of Symmetry, *Phys. Rev. X* **5**, 011005 (2015).
- [9] M. Pósfai, J. Gao, S. P. Cornelius, A.-L. Barabási, and R. M. D'Souza, Controllability of multiplex, multi-time-scale networks, *Phys. Rev. E* **94**, 032316 (2016).
- [10] X. Liu, L. Pan, H. E. Stanley, and J. Gao, Controllability of giant connected components in a directed network, *Phys. Rev. E* **95**, 042318 (2017).
- [11] I. Klickstein, A. Shirin, and F. Sorrentino, Locally Optimal Control of Complex Networks, *Phys. Rev. Lett.* **119**, 268301 (2017).
- [12] G. Li, L. Deng, G. Xiao, P. Tang, C. Wen, W. Hu, J. Pei, L. Shi, and H. E. Stanley, Enabling controlling complex networks with local topological information, *Sci. Rep.* **8**, 4593 (2018).
- [13] J.-H. Zhao and H.-J. Zhou, Controllability and maximum matchings of complex networks, *Phys. Rev. E* **99**, 012317 (2019).
- [14] J. Jiang and Y.-C. Lai, Irrelevance of linear controllability to nonlinear dynamical networks, *Nat. Commun.* **10**, 3961 (2019).
- [15] R. Albert and A.-L. Barabási, Statistical mechanics of complex networks, *Rev. Mod. Phys.* **74**, 47 (2002).
- [16] I. Rajapakse, M. Groudine, and M. Mesbahi, Dynamics and control of state-dependent networks for probing genomic organization, *Proc. Natl. Acad. Sci. U.S.A.* **108**, 17257 (2011).
- [17] G. Yan, P. E. Vértes, E. K. Towilson, Y. L. Chew, D. S. Walker, W. R. Schafer, and A.-L. Barabási, Network control principles predict neuron function in the *Caenorhabditis elegans* connectome, *Nature* **550**, 519 (2017).
- [18] Y. N. Kenett, R. E. Beaty, and J. D. Medaglia, A computational network control theory analysis of depression symptoms, *Personal. Neurosci.* **1**, E16 (2018).
- [19] H. Zhang, X. Liu, Q. Wang, W. Zhang, and J. Gao, Coadaptation enhances the resilience of mutualistic networks, *J. R. Soc. Interface* **17**, 20200236 (2020).
- [20] J. Ruths and D. Ruths, Control profiles of complex networks, *Science* **343**, 1373 (2014).
- [21] D. Delpini, S. Battiston, M. Riccaboni, G. Gabbi, F. Pammolli, and G. Caldarelli, Evolution of controllability in interbank networks, *Sci. Rep.* **3**, 1626 (2013).
- [22] C. Castellano, S. Fortunato, and V. Loreto, Statistical physics of social dynamics, *Rev. Mod. Phys.* **81**, 591 (2009).
- [23] Z. Yuan, C. Zhao, Z. Di, W.-X. Wang, and Y.-C. Lai, Exact controllability of complex networks, *Nat. Commun.* **4**, 2447 (2013).
- [24] G. Yan, J. Ren, Y.-C. Lai, C.-H. Lai, and B. Li, Controlling Complex Networks: How Much Energy is Needed? *Phys. Rev. Lett.* **108**, 218703 (2012).
- [25] G. Li, W. Hu, G. Xiao, L. Deng, P. Tang, J. Pei, and L. Shi, Minimum-cost control of complex networks, *New J. Phys.* **18**, 013012 (2015).
- [26] G. Lindmark and C. Altafini, Minimum energy control for complex networks, *Sci. Rep.* **8**, 3188 (2018).
- [27] J. Ding, C. Wen, G. Li, and Z. Chen, Key nodes selection in controlling complex networks via convex optimization, *IEEE Trans. Cybernet.* **51**, 52 (2019).
- [28] H. Chen and E. H. Yong, Optimizing target nodes selection for the control energy of directed complex networks, *Sci. Rep.* **10**, 18112 (2020).
- [29] Y.-Z. Chen, L.-Z. Wang, W.-X. Wang, and Y.-C. Lai, Energy scaling and reduction in controlling complex networks, *R. Soc. Open Sci.* **3**, 160064 (2016).
- [30] L.-Z. Wang, Y.-Z. Chen, W.-X. Wang, and Y.-C. Lai, Physical controllability of complex networks, *Sci. Rep.* **7**, 40198 (2017).
- [31] G. Yan, G. Tsekenis, B. Barzel, J.-J. Slotine, Y.-Y. Liu, and A.-L. Barabási, Spectrum of controlling and observing complex networks, *Nat. Phys.* **11**, 779 (2015).
- [32] I. Klickstein, A. Shirin, and F. Sorrentino, Energy scaling of targeted optimal control of complex networks, *Nat. Commun.* **8**, 15145 (2017).
- [33] G. Duan, A. Li, T. Meng, G. Zhang, and L. Wang, Energy cost for controlling complex networks with linear dynamics, *Phys. Rev. E* **99**, 052305 (2019).
- [34] G. Duan, A. Li, T. Meng, and L. Wang, Energy cost for target control of complex networks, *Adv. Complex Syst.* **22**, 1950022 (2019).
- [35] D. Madeo and C. Mocenni, Self-regulation versus social influence for promoting cooperation on networks, *Sci. Rep.* **10**, 4830 (2020).
- [36] X.-W. Wang, S. Nie, W.-X. Wang, and B.-H. Wang, Controlling complex networks with conformity behavior, *Europhys. Lett.* **111**, 68004 (2015).
- [37] J.-J. Wu, C. Li, B.-Y. Zhang, R. Cressman, and Y. Tao, The role of institutional incentives and the exemplar in promoting cooperation, *Sci. Rep.* **4**, 6421 (2014).
- [38] E. Van de Waal, C. Borgeaud, and A. Whiten, Potent social learning and conformity shape a wild primate's foraging decisions, *Science* **340**, 483 (2013).
- [39] A. Whiten, V. Horner, and F. B. De Waal, Conformity to cultural norms of tool use in chimpanzees, *Nature* **437**, 737 (2005).
- [40] T. Vicsek and A. Zafeiris, Collective motion, *Phys. Rep.* **517**, 71 (2012).
- [41] T. Vicsek, A. Czirók, E. Ben-Jacob, I. Cohen, and O. Shochet, Novel Type of Phase Transition in a System of Self-Driven Particles, *Phys. Rev. Lett.* **75**, 1226 (1995).
- [42] M. Nagy, Z. Ákos, D. Biro, and T. Vicsek, Hierarchical group dynamics in pigeon flocks, *Nature* **464**, 890 (2010).

- [43] A. J. Ward, D. J. Sumpter, I. D. Couzin, P. J. Hart, and J. Krause, Quorum decision-making facilitates information transfer in fish shoals, *Proc. Natl. Acad. Sci. U.S.A.* **105**, 6948 (2008).
- [44] J. Buhl, D. J. Sumpter, I. D. Couzin, J. J. Hale, E. Despland, E. R. Miller, and S. J. Simpson, From disorder to order in marching locusts, *Science* **312**, 1402 (2006).
- [45] D. Acemoglu, A. Ozdaglar, and A. ParandehGheibi, Spread of (mis)information in social networks, *Games Econ. Behav.* **70**, 194 (2010).
- [46] M. Perc, J. Gómez-Gardenes, A. Szolnoki, L. M. Floría, and Y. Moreno, Evolutionary dynamics of group interactions on structured populations: A review, *J. R. Soc. Interface* **10**, 20120997 (2013).
- [47] M. Perc and A. Szolnoki, Coevolutionary games—A mini review, *BioSystems* **99**, 109 (2010).
- [48] C. Hilbe, B. Wu, A. Traulsen, and M. A. Nowak, Cooperation and control in multiplayer social dilemmas, *Proc. Natl. Acad. Sci. U.S.A.* **111**, 16425 (2014).
- [49] F. L. Lewis and V. L. Syrmos, *Optimal Control*, 3rd ed. (Wiley, New York, 1995).
- [50] A. Li, S. P. Cornelius, Y.-Y. Liu, L. Wang, and A.-L. Barabási, Control energy scaling in temporal networks, [arXiv:1712.06434](https://arxiv.org/abs/1712.06434) (2017).
- [51] A. Li, S. P. Cornelius, Y.-Y. Liu, L. Wang, and A.-L. Barabási, The fundamental advantages of temporal networks, *Science* **358**, 1042 (2017).
- [52] R. A. Horn and C. R. Johnson, *Matrix Analysis* (Cambridge University Press, Cambridge, UK, 2012).
- [53] See Supplemental Material at <http://link.aps.org/supplemental/10.1103/PhysRevE.104.014301> for analytical equations derivation, which includes Refs. [34,49,56–58,66].
- [54] J. Lam, Z. Li, Y. Wei, J.-e. Feng, and K. W. Chung, Estimates of the spectral condition number, *Lin. Multilin. Alg.* **59**, 249 (2011).
- [55] C.-T. Chen, *Linear System Theory and Design* (Oxford University Press, Oxford, UK 1999).
- [56] H. R. Bernard, P. D. Killworth, and L. Sailer, Informant accuracy in social network data IV: A comparison of clique-level structure in behavioral and cognitive network data, *Soc. Netw.* **2**, 191 (1979).
- [57] W. W. Zachary, An information flow model for conflict and fission in small groups, *J. Anthropol. Res.* **33**, 452 (1977).
- [58] K. B. Petersen and M. S. Pedersen, The matrix cookbook, Nov. 2012, <http://www2.imm.dtu.dk/pubdb/p.php> (2012).
- [59] W. J. Rugh, *Linear System Theory* (Prentice-Hall, Hoboken, NJ, 1996).
- [60] K.-I. Goh, B. Kahng, and D. Kim, Universal Behavior of Load Distribution in Scale-Free Networks, *Phys. Rev. Lett.* **87**, 278701 (2001).
- [61] J. C. Nacher and T. Akutsu, Dominating scale-free networks with variable scaling exponent: Heterogeneous networks are not difficult to control, *New J. Phys.* **14**, 073005 (2012).
- [62] S. M. Krause, F. Weyhausen-Brinkmann, and S. Bornholdt, Repulsion in controversial debate drives public opinion into fifty-fifty stalemate, *Phys. Rev. E* **100**, 042307 (2019).
- [63] F. Baumann, P. Lorenz-Spreen, I. M. Sokolov, and M. Starnini, Modeling Echo Chambers and Polarization Dynamics in Social Networks, *Phys. Rev. Lett.* **124**, 048301 (2020).
- [64] Advanpix llc. multiprecision computing toolbox for matlab v.4.8.0.14105. <http://www.advanpix.com> (2020).
- [65] T. P. Patel, K. Man, B. L. Firestein, and D. F. Meaney, Automated quantification of neuronal networks and single-cell calcium dynamics using calcium imaging, *J. Neurosci. Methods* **243**, 26 (2015).
- [66] <http://moreno.ss.uci.edu/data.html>.